High-temperature noncollinear magnetism in a classical bilinear-biquadratic Heisenberg model

Kanika Pasrija and Sanjeev Kumar
Indian Institute of Science Education and Research (IISER) Mohali, Knowledge City, Sector 81, Mohali 140 306, India
(Received 13 August 2013; published 21 October 2013)

Motivated by the magnetically driven high-temperature ferroelectric behavior of CuO and the subsequent theoretical efforts to understand this intriguing phenomenon, we study a bilinear-biquadratic Heisenberg model on a two-dimensional square lattice, which possesses some of the key features of the models proposed for CuO. We use a combination of variational calculations and classical Monte Carlo simulations to study this model at zero and finite temperatures. We show that the biquadratic coupling plays a crucial role in selecting the magnetic ground state. More importantly, a noncollinear magnetic state is found to be stable at finite temperatures. Our study demonstrates that higher-order interaction terms are of crucial importance if the stronger interactions together with the lattice geometry combine to generate a near degeneracy of magnetic states.

DOI: 10.1103/PhysRevB.88.144418 PACS number(s): 75.10.Hk, 75.40.Mg, 75.85.+t, 75.47.Lx

I. INTRODUCTION

Materials exhibiting more than one ferroic ordering phenomena in a single phase are defined as multiferroics.[1] Over the last few years, magnetoelectric multiferroics have received a special attention from solid-state and materials researchers for the exciting possibility of designing powerful memory devices, where an electrical writing and a nondestructive magnetic reading is allowed.[2–5] It was soon realized that there is a scarcity of materials that simultaneously exhibit ferroelectricity and ferromagnetism.[6,7] In fact, it appeared that a ferroelectric order rarely coexists with any long-range magnetic order.[8,9] This was attributed to the fact that ferroelectric materials typically have a d^0 electronic configuration, whereas it is the partial filling of d levels that is responsible for magnetism in a large number of compounds. Following this observation researchers started to search for materials that are exceptions to this rule. Over the course of last decade, the original definition of magnetoelectric multiferroic order has been extended to include materials which exhibit ferroelectric order together with any long-range magnetic order.[10] Within this new definition of multiferroics, a large class of new multiferroic compounds have been discovered, which range from transition-metal oxides to organic crystals.[11–17] On the theoretical side, many new mechanisms were proposed that allow the ferroelectric order to coexist with a magnetic order.[18–21]

For practical applications, the multiferroic phase should be stable at room temperature, and the coupling between ferroelectric and magnetic order parameters should be strong. Although, the most well known multiferroic, $BiFeO_3$, has large magnetic and ferroelectric ordering temperatures, the coupling between the two order parameters is rather weak.[22] This is due to the fact that the magnetism in $BiFeO_3$ comes from the Fe, whereas ferroelectricity arises due to off centering of the Bi ions. On the other hand, strong magnetoelectric coupling was discovered in some systems with a spiral-type long-range magnetic order, where the ferroelectricity is induced by the spin-spiral states.[23] Therefore, one way of ensuring a strong coupling between magnetic and ferroelectric order parameters is to look for materials where ferroelectricity emerges as a consequence of some magnetic order, such as the spin-spiral states. There are various mechanisms that can lead to the existence of such magnetic states, e.g., magnetic frustration in strongly correlated Mott insulators, the Dzyaloshinskii-Moriya (DM) interactions, etc.[24,25] Typically, such spin-spiral states are stable only at low temperatures. Cupric oxide (CuO) emerges as a promising candidate, which possesses the two main features of an ideal multiferroic: (i) high ordering temperature and (ii) magnetism induced ferroelectricity.[26–28]

A number of theoretical investigations have been reported since the discovery of high-temperature ferroelectricity in CuO.[29–32] It has been established that the magnetic interactions in CuO are rather complicated, and lead to competing ground states. There is still no consensus on the experimental values of the various exchange parameters.[33–35] Similarly, the outcome of the theoretical calculations of the exchange parameters depend on the details of the method used.[29,32,36] Nevertheless, most theoretical models point to a near degeneracy of magnetic states in this system. Giovannetti *et al.* proposed that the competition between a small uniaxial anisotropy and weak DM interactions leads to the observed experimental behavior of the ferroelectric polarization.[29] The model was further improved by Jin *et al.* by explicitly including the lattice parameters in the microscopic Hamiltonian.[30] Both these studies point towards a crucial role played by entropic effects in stabilizing the noncollinear magnetic phase at high temperatures.

In this work we explore some features of the magnetic ordering phenomena in CuO without taking into account the detailed crystal structure of the material. In order to keep the scope of this work general we use a simple two-dimensional (2D) square lattice with nearest- and next-nearest-neighbor magnetic exchange couplings. The model does not include an explicit symmetry-breaking term such as a DM interaction, however it includes higher-order spin-spin interaction terms. Although the strength of the higher-order terms is much weaker than the Heisenberg exchange terms, the former become important due to near degeneracy of states in the pure Heisenberg model. We present extensive Monte Carlo simulation results on a 2D bilinear-biquadratic (BLBQ) Heisenberg model. We find that the biquadratic coupling drives a first-order phase transition between a collinear up-up-down-down type antiferromagnet (denoted as EAF) and a spiral antiferromagnet at low temperatures. At finite temperatures the noncollinear phase is found to be more stable compared to the collinear phase. This leads to a sequence of phase transitions from a

high-temperature paramagnetic state to a noncollinear state, and finally to a collinear EAF phase at low temperatures. This is precisely the behavior reported in the experimental studies of CuO. We find that a pure electronic Hamiltonian is sufficient to describe the magnetism in CuO provided higher-order interaction terms are taken into account. While our model study is of general importance for magnetic materials and models, the conclusions are of particular relevance to the magnetic and ferroelectric ordering phenomena in CuO.

The rest of the paper is organized as follows. In Sec. II we describe possible extensions of the standard Heisenberg model for spin-1/2 and spin-1 magnetic moments. We discuss the relevance of these models and their relation with each other in the classical limit. Section II ends with a description of the variational, and Monte Carlo (MC) simulation methods used in this work. Section III begins with a discussion of the ground-state phase diagrams of the two models using variational calculations. Next, a comparison between variational calculations and MC simulations at low temperatures is presented. Finally, the finite-temperature behavior of the BLBQ model is discussed. The main focus is on the presence of a noncollinear magnetic phase with finite electric polarization at high temperatures. Conclusions are presented in Sec. IV.

II. MODEL AND METHOD

We begin with a Heisenberg Hamiltonian on a square lattice given by

$$H_0 = J_1 \sum_{\langle ij\rangle} \mathbf{S}_i \cdot \mathbf{S}_j + J_{2a} \sum_{\langle\langle ij\rangle\rangle_a} \mathbf{S}_i \cdot \mathbf{S}_j + J_{2b} \sum_{\langle\langle ij\rangle\rangle_b} \mathbf{S}_i \cdot \mathbf{S}_j.$$

Here, J_1 denotes the nearest-neighbor (nn) Heisenberg exchange coupling and J_{2a}, J_{2b} are the next-nearest-neighbor (nnn) couplings as shown in Fig. 1(a). The single and double angular brackets denote the sum over nn and nnn sites, respectively. The subscripts a and b on the summation indices specify the two inequivalent nnn directions. For most spin systems with square lattice geometry, one is typically interested in the parameter regime given by, $|J_{2a}| \sim |J_{2b}| \leqslant |J_1|$. However, another interesting limit of this model is realized when J_{2a} and J_{2b} have opposite signs and are much larger in magnitude compared to $|J_1|$. The corresponding model for Ising spins was recently analyzed by A. Kalz and G. Chitov, and the existence

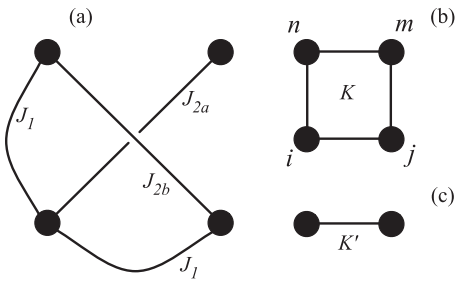

FIG. 1. Schematic representation of various interactions that constitute the model Hamiltonians H_1 and H_2 discussed in the text. (a) The nearest-neighbor, and the next-nearest-neighbor Heisenberg exchange couplings on a square lattice, (b) the four-spin ring-exchange coupling in Hamiltonian Eq. (2), and (c) the biquadratic coupling in Hamiltonian Eq. (3).

of an unusual topological floating phase was reported.[37] It is easy to see that in this limit, the magnetic system gets divided into two sublattices, which interpenetrate each other. J_{2a} and J_{2b} ensure that each sublattice has a well defined order at low temperatures, but the nn Heisenberg coupling J_1 is not sufficient to generate a long-range magnetic order. Therefore, in this parameter regime higher-order spin-spin interaction terms become relevant. Interestingly, the magnetic model for CuO corresponds to a similar sublattice order in three dimensions where each sublattice has a well defined order but the magnetic ground state is degenerate and additional weaker couplings, such as the magnetocrystalline anisotropy and the Dzyaloshinskii-Moriya (DM) interaction, are considered important. However, the higher-order spin-spin interactions should be given equal importance in this regime. Proceeding with this viewpoint, our first extension of the Heisenberg Hamiltonian H_0 is achieved by including a four-spin ring-exchange interaction, leading to the Hamiltonian,

$$H_1 = H_0 + K \sum_{[ijmn]} [(\mathbf{S}_i \cdot \mathbf{S}_j)(\mathbf{S}_m \cdot \mathbf{S}_n) + (\mathbf{S}_i \cdot \mathbf{S}_n)(\mathbf{S}_j \cdot \mathbf{S}_m) - (\mathbf{S}_i \cdot \mathbf{S}_m)(\mathbf{S}_j \cdot \mathbf{S}_n)]. \quad (1)$$

In the above, K denotes the strength of the ring-exchange coupling involving four sites [see Fig. 1(b)]. Starting with a one-band Hubbard model at half-filling, the second-order perturbation theory in hopping leads to the Heisenberg exchange.[38] If we go beyond the second order, the next contribution is from the fourth-order term leading to the ring-exchange coupling.[39] Therefore, H_1 is the microscopic Hamiltonian for spin-1/2 moments on a square lattice. If the magnetic moments are spin-1, then the next order term is a biquadratic one involving two sites.[40] Note that a biquadratic coupling term in the effective classical action can also arise as a result of quantum fluctuations even in a spin-1/2 system.[41] We define our second Hamiltonian, H_2, by including a biquadratic term to H_0. The Hamiltonian is given by

$$H_2 = H_0 + K' \sum_{\langle ij\rangle_x} (\mathbf{S}_i \cdot \mathbf{S}_j)^2. \quad (2)$$

Here, K' is the coupling strength of the biquadratic interaction, which we have taken to be present only on the nn bond along the x direction [see Fig. 1(c)].

H_1 (H_2) is the spin Hamiltonian containing interaction terms up to fourth order for spin-1/2 (spin-1) magnetic moments. However, in the classical limit these two models have many similarities. This is particularly easy to recognize when J_{2a} and J_{2b} are stronger couplings compared to J_1. The term inside the square brackets in Eq. (2) can be rewritten as $[(\mathbf{S}_i \cdot \mathbf{S}_j)(\mathbf{S}_m \cdot \mathbf{S}_n) - (\mathbf{S}_i \times \mathbf{S}_j) \cdot (\mathbf{S}_m \times \mathbf{S}_n)]$. Now given that the nnn couplings are much stronger, at low temperatures $\mathbf{S}_i$ ($\mathbf{S}_j$) is either parallel or antiparallel to $\mathbf{S}_m$ ($\mathbf{S}_n$), depending on the sign of J_{2a} (J_{2b}). Making the substitutions $\mathbf{S}_m \to \mathbf{S}_i$ and $\mathbf{S}_n \to \mathbf{S}_j$, we can rewrite H_1 as

$$H_1 = H_0 + K \sum_{\langle ij\rangle} [(\mathbf{S}_i \cdot \mathbf{S}_j)^2 - (\mathbf{S}_i \times \mathbf{S}_j)^2]. \quad (3)$$

We finally note that $(\mathbf{S}_i \times \mathbf{S}_j)^2 = |S|^4 - (\mathbf{S}_i \cdot \mathbf{S}_j)^2$, and therefore the two models H_1 and H_2 are identical up to an additive constant and the sign of the coupling constant. The

equivalence of these two Hamiltonians is valid only in the classical limit, and at temperatures scales much smaller than the nnn coupling strengths.

The BLBQ Heisenberg model has been well studied as a quantum spin-1 Hamiltonian on various lattices.[42–44] The model has also been studied recently in the classical limit,[45] where the focus was on the existence of noncoplanar phases, and the ground-state degeneracies on a triangular lattice. There is also a study on pyrochlore lattice in the context of Cr spinels and their magnetic properties.[46] In addition, there have been numerous studies trying to understand the properties of quantum spin chains using a variety of theoretical methods.[47] In this paper, we study the BLBQ Heisenberg Hamiltonian as a candidate for noncollinear magnetism at high temperatures in systems where the pure Heisenberg term leads to degenerate ground states.

In the next section we compare the classical ground-state phase diagrams of the two Hamiltonians, H_1 and H_2. The parameters of the models are, J_1, J_{2a}, J_{2b}, and $K(K')$. Since we are interested in the regime where nnn couplings are stronger than nn ones, we set $J_{2a} = 1$ as our energy scale, and all other couplings and energies are therefore expressed in terms of J_{2a}. In order to compare the ground-state phase diagrams of the two models described by H_1 and H_2, we use a variational scheme. We consider planar spiral spin states with spiral wave vector $\mathbf{q} = (q_x, q_y)$. The orientation of the magnetic moment at lattice site $\mathbf{r}_i$ is given by, $\mathbf{S}_i = |S|(\cos(\mathbf{q}\cdot\mathbf{r}_i), \sin(\mathbf{q}\cdot\mathbf{r}_i), 0)$. Such spiral states contain the conventional magnetically ordered states, such as the ferromagnet, staggered antiferromagnet, stripe-type antiferromagnet and orthogonal state as limiting cases (see Fig. 2). We minimize the total energy of a general spiral state for different values of model parameters. In addition, we include two more states in our minimization scheme. These are the so-called flux state and the up-up-down-down type antiferromagnet (EAF) state (see Fig. 2). We make use of MATHEMATICA for performing the variational minimization described above.

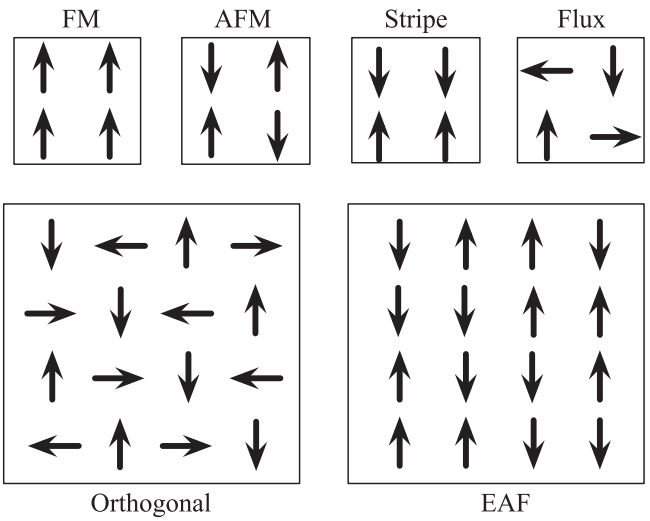

FIG. 2. Schematic view of various magnetically ordered states considered in the variational calculations. A general spiral phase is not shown here. The ferromagnet, antiferromagnet, stripe, and orthogonal phases are limiting cases of spiral states with $q_x = q_y = 0$ (FM), $q_x = q_y = \pi$ (AFM), $q_x = 0, q_y = \pi$ (stripe), and $q_x = q_y = \pi/2$ (orthogonal). The flux phase and the up-up-down-down type antiferromagnet, EAF, do not belong to the set of spiral states.

Classical Monte Carlo simulations are employed for the finite-temperature study of the BLBQ Hamiltonian.[48] The standard Markov chain Monte Carlo method is used with the METROPOLIS algorithm for configuration updates.[49] Single-spin update moves are performed by randomly selecting a pair of polar and azimuthal angles for a given spin. The move is accepted with the Boltzmann probability $e^{-\Delta E/(k_B T)}$, where ΔE is the energy difference between the new and the old configurations, T is the temperature and k_B is the Boltzmann constant. Following the standard practice in such simulations, we set $k_B = 1$ so that the temperature scales become equivalent to the energy scales. Each spin is updated $N_{\rm eq} \sim 10^6$ times for the purpose of thermalization of the system. Thereafter, we begin to compute physical quantities, which are averaged over $N_{\rm av} \sim 10^6$ further update steps. Most of the results are presented on a square lattice with 120^2 spins. However, the stability of results is checked on lattice sizes varying from 80^2 to 200^2 for selected parameter values.

III. RESULTS AND DISCUSSIONS

A. Ground-state phase diagrams

We begin by presenting the classical ground-state phase diagrams for the Hamiltonian Eq. (2). Due to the presence of a four-spin interaction term, the standard method of Luttinger and Tisza for finding the ground states of a classical spin Hamiltonian does not work.[50] Therefore, we rely on variational calculation for determining the ground-state magnetic phases of the model. We consider the general spiral states, the up-up-down-down type antiferromagnetic (EAF) state and the flux state, as described in the previous section. We also allowed for spiral states with a finite ferromagnetic moment, but such phases were not stable for any combination of the parameter values explored. A schematic view of the different ordering patterns considered in our variational calculations is shown in Fig. 2. The phase diagrams are obtained by minimizing the energy of the system over these states. As mentioned earlier, we set $J_{2a} = 1$ as the reference energy scale. Therefore the free parameters to be explored are J_1, J_{2b} and K.

The energy per spin for various ordered magnetic states for the Hamiltonian Eq. (2) is given by the following equations:

$$E_{\rm EAF} = -J_{2a} + J_{2b} - K, \tag{4}$$

$$\begin{aligned} E_{\rm Spiral} = {} & J_1(\cos q_x + \cos q_y) + J_{2a}\cos(q_x + q_y) \\ & + J_{2b}\cos(q_x - q_y) + K[\cos^2 q_x + \cos^2 q_y \\ & - \cos(q_x + q_y)\cos(q_x - q_y)], \end{aligned} \tag{5}$$

$$E_{\rm Flux} = -J_{2a} - J_{2b} - K. \tag{6}$$

In Fig. 3, we show the J_1-J_{2b} phase diagrams for two values of the ring-exchange coupling strength K. The different phases are indicated with acronyms in the figure. For negative values of K, all ground-state phases are of spiral type. The region denoted as Spiral in the phase diagram consists of spiral phases with $q_x = q_y$. The FM state is continuously connected to AFM via the spiral states. For positive values of K, the flux state and

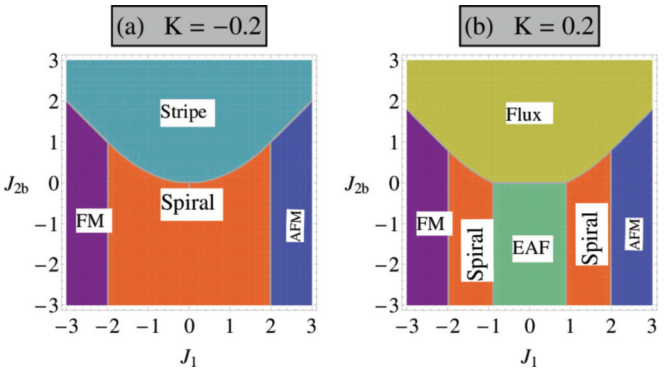

FIG. 3. (Color online) J_1-J_{2b} ground-state phase diagram of the Hamiltonian H_1 for the ring-exchange coupling values, (a) $K = -0.2$ and (b) $K = 0.2$. For $K = -0.2$ and $J_{2b} < 0$, the FM phase continuously evolves to a staggered antiferromagnetic phase via spin-spiral magnetic states with the wave vector following the condition $q_x = q_y$.

the EAF state occupy a considerable region of the parameter space. The boundaries between the spiral phase and the EAF phase are first order in nature since the order parameter of one phase is not continuously connected to that of the other. The two most relevant phases are the EAF and the orthogonal (spiral with $q_x = q_y = \pi/2$) phase. These are the 2D analogs of the collinear AF_1 and noncollinear AF_2 states observed in CuO.[26] In Fig. 4, we show the K-J_{2b} phase diagrams at two values of the nearest-neighbor coupling J_1. The four stable phases are almost symmetrically placed in four quadrants for a small value of J_1. Increasing J_1 leads to an enhanced stability of the spiral phase.

Having discussed the phase diagrams for the Hamiltonian with ring-exchange coupling, we now turn to the BLBQ Hamiltonian specified by Eq. (3). The expressions for energy per spin of different ordered states is given by the following equations:

$$E_{\mathrm{EAF}} = -J_{2a} + J_{2b} + K', \tag{7}$$

$$E_{\mathrm{Spiral}} = J_1(\cos q_x + \cos q_y) + J_{2a}\cos(q_x + q_y) + J_{2b}\cos(q_x - q_y) + K'\cos^2 q_x, \tag{8}$$

$$E_{\mathrm{Flux}} = -J_{2a} - J_{2b}. \tag{9}$$

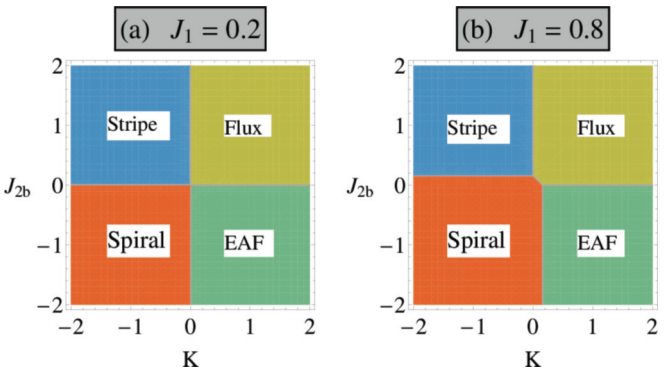

FIG. 4. (Color online) K-J_{2b} ground-state phase diagram of the Hamiltonian H_1 for two values of the nn Heisenberg exchange coupling, (a) $J_1 = 0.2$ and (b) $J_1 = 0.8$.

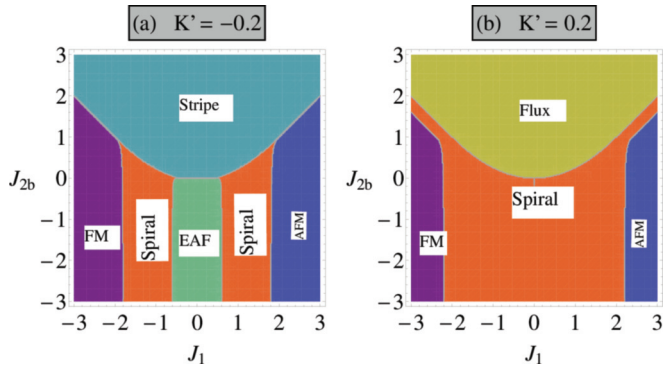

FIG. 5. (Color online) J_1-J_{2b} ground-state phase diagram of the Hamiltonian H_2 for two values of the biquadratic coupling strength, (a) $K' = -0.2$ and (b) $K' = 0.2$. Note the similarity with the phase diagram shown in Fig. 3.

Once again, we use a variational approach to obtain the phase diagrams. The model parameters in this case are J_1, J_{2b}, and K'. In Fig. 5, we show the J_1-J_{2b} phase diagrams at two values of the biquadratic coupling strength K'. The different phases are again indicated with acronyms in the figure. There is a remarkable similarity between these phase diagrams and those shown in Fig. 3. Both sets of phase diagrams contain identical phases with almost identically located phase boundaries, except for a relative sign between the couplings K and K' for negative J_{2b} as discussed in Sec. II. Once again, the relevant phases having collinear and noncollinear magnetic orders are part of the ground-state phase diagram.

To complete the comparison we present the K'-J_{2b} phase diagram for two values of J_1 in Fig. 6. Once again the phase diagrams contain the same four phases as shown in Fig. 4. In addition, increasing J_1 leads to an expansion of the stability regime for the spiral states. Note that spin nematic states can exist for large value of biquadratic couplings, however this parameter regime is beyond the scope of the present work. Moreover, such states cannot be captured within the methods used here.[51]

The variational results highlight the rich behavior of the models H_1 and H_2 in terms of the presence of a variety of phases and phase boundaries. The results further suggest that while the form of higher-order spin-spin interactions arising

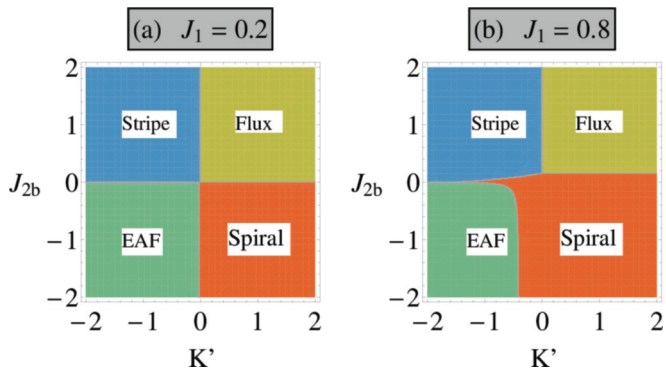

FIG. 6. (Color online) K'-J_{2b} ground-state phase diagram of the BLBQ Hamiltonian H_2 for, (a) $J_1 = 0.2$ and (b) $J_1 = 0.8$. Similarity with the phase diagrams shown in Fig. 4 is apparent.

from a strong-coupling expansion is different for spin-1/2 and spin-1 magnetic moments, their classical versions lead to phase diagrams with strong similarities. Given that the BLBQ Hamiltonian has a simple form with each term containing pairwise interactions between spins, we select H_2 for finite-temperature studies. We now proceed to study H_2 in more detail. Our main aim is to understand the finite-temperature behavior of a Heisenberg model whose ground-state degeneracy is lifted by a higher-order spin-spin coupling term.

B. Comparison between variational and Monte Carlo results

The variational phase diagrams discussed in the previous subsection show that the model contains a variety of phases and phase transitions in the ground state. In order to ensure that we have not missed any crucial magnetic state in our variational setup, we verify the stability of some of these phases using Monte Carlo simulations. The details of the method are given in Sec. II. We present the Monte Carlo results on the BLBQ Hamiltonian given by Eq. (3). Various quantities calculated in the Monte Carlo simulations are defined in the following. The total energy per spin, $E = \frac{1}{N}\langle H\rangle$, is computed by taking the thermal average of the Hamiltonian over the Monte Carlo-generated finite-temperature configurations. Here onwards, the angular brackets denote thermal average, which for any quantity X is defined as

$$\langle X\rangle = \frac{1}{N_{\rm av}}\sum_{\alpha=1}^{N_{\rm av}} X_\alpha, \tag{10}$$

where α denotes a single configuration with X_α being the value of the quantity X for that configuration and $N_{\rm av}$ is the number of MC steps over which the averaging is performed. In order to characterize the various magnetic states, we compute the spin-structure factor,

$$S(\mathbf{q}) = \frac{1}{N}\sum_{ij} e^{-i\mathbf{q}\cdot(\mathbf{r}_i-\mathbf{r}_j)}\langle \mathbf{S}_i\cdot\mathbf{S}_j\rangle, \tag{11}$$

where $\mathbf{r}_i$ denotes the real-space coordinate of the spin $\mathbf{S}_i$, N is the number of total spins, and the sum is over all pairs of spins. The spiral states are characterized by a peak in $S(\mathbf{q})$ at a single value of $\mathbf{q}$. The corresponding value of $\mathbf{q}$ is the spiral wave vector. In fact, the nn dot product is another useful quantity in this context. We define a general $\mathbf{Q}$ average of the dot product as

$$D_x(\mathbf{Q}) = \frac{1}{N}\left\langle\left|\sum_i e^{i\mathbf{Q}\cdot\mathbf{r}_i}\mathbf{S}_i\cdot\mathbf{S}_{i+\hat{x}}\right|\right\rangle, \tag{12}$$

where the vertical bars denote the absolute value, and $\mathbf{S}_{i+\hat{x}}$ is the nn spin of $\mathbf{S}_i$ along x direction on the square lattice. One can similarly define $D_y(\mathbf{Q})$. If the system is in a spiral phase, then $D_x(\mathbf{Q})$ at $\mathbf{Q} = (0,0)$ (denoted as $D_x(0)$ here onwards) is finite and serves as an order parameter for the spiral state. The x and y components of the spiral wave vectors can be directly computed as $q_{x/y} = \cos^{-1}[D_{x/y}(0)]$. Note that a canted state will not be distinguished from a spiral by using only $D_{x/y}(0)$, therefore it is important to keep track of the spin-structure factor $S(\mathbf{q})$. In the EAF phase, $D_x(0) = 0$ in the same way as the net magnetization is zero in the AFM.

We begin by taking a single scan along the J_1 axis from the phase diagrams presented in Fig. 5 at a fixed value of $J_{2b} = -1$. For $K' = -0.2$, the variational phase diagram suggests a transition from a FM to AFM state via a spiral state and an EAF state. On the other hand, for $K' = 0.2$ the EAF state does not appear. We perform Monte Carlo simulations at constant low temperature ($T = 0.02$) for the above choice of parameters. We start with a FM state at $J_1 = -2$ and increase the nn coupling constant up to $J_1 = 2$ in steps of 0.02. The energy per spin and $D_x(0)$ are tracked as a function of J_1. We then begin with an AFM state at $J_1 = 2$ and trace back to $J_1 = -2$. Tracing forward and backward in J_1 allows us to probe the hysteresis behavior in the system. The results are presented in Fig. 7. Since the order parameter for a spiral state does not evolve continuously to that of an EAF state a hysteresis is present in the computed physical quantities [see Figs. 7(a) and 7(c)]. Indeed, according to the variational phase diagram the regime of EAF state is between $-0.6 < J_1 < 0.6$, which is well captured by the Monte Carlo results. The EAF phase is absent in the phase diagram for $K' = 0.2$, and therefore the spiral state connects a FM [spiral with wave vector $(0,0)$] continuously to an AFM [spiral with wave vector (π,π)], hence no hysteresis behavior is found in Figs. 7(b) and 7(d). In order to make these comparisons quantitative, we plot $D_x(0)$ obtained from variational calculations (blue circles in Fig. 7). Monte Carlo simulations performed directly at low temperature accurately capture the variational results.

The above checks confirm the validity of ground-state phase diagrams obtained via the variational method. They also serve as a benchmark for the efficiency of our Monte Carlo simulations. In addition to the above checks, we also compared

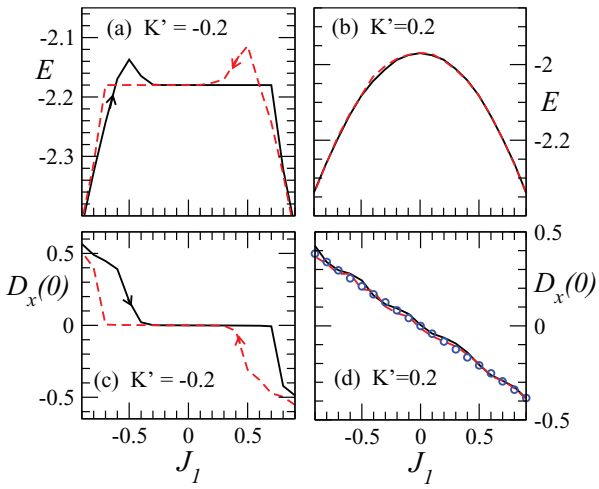

FIG. 7. (Color online) Energy per spin obtained via Monte Carlo simulations, plotted as a function of the nn coupling strength J_1 for (a) $K' = -0.2$ and (b) $K' = 0.2$. Thermally averaged dot product of neighboring spins, $D_x(0)$ (defined in text) as a function of J_1 for (c) $K' = -0.2$ and (d) $K' = 0.2$. The simulations are carried out at $J_{2b} = -1$ and at a fixed temperature $T = 0.02$, by increasing (solid lines) and decreasing (dashed lines) the parameter J_1. The hysteresis in (a) and (c) is an indicator of a first-order phase transition, whereas the absence of hysteresis in (b) and (d) suggests a smooth crossover from FM to AFM via the spiral states. Circles in (d) are the corresponding values obtained from variational calculations.

TABLE I. Comparison of energy per spin obtained in variational calculations and that obtained in Monte Carlo simulations at low temperature ($T = 0.005$), for different choices of parameter sets. The comparison shows that the variational scheme is able to correctly describe the various ground-state phase boundaries within the classical approximation.

Parameters ⇓ / Energies ⇒	E_{MC}	E_{var}
$J_1 = -0.1,\ J_{2b} = +1.0,\ K' = -0.2$	−2.195	−2.200
$J_1 = -0.1,\ J_{2b} = -1.0,\ K' = -0.2$	−2.195	−2.200
$J_1 = -1.5,\ J_{2b} = -1.0,\ K' = -0.2$	−3.167	−3.237
$J_1 = -0.1,\ J_{2b} = +1.0,\ K' = +0.2$	−1.995	−2.000

the energies obtained from the MC at low temperatures ($T = 0.005$) with those obtained in the variational calculations, for different choices of parameters belonging to different ground state magnetic phases. These energy comparisons are shown in Table I.

The energies compare very well between the Monte Carlo simulations and the variational calculations. We also verify using the spin-structure factor $S(\mathbf{q})$ that the ordered phases obtained in the MC are same as those shown in the variational phase diagrams for each choice of the parameter sets listed in Table I.

Having established a correspondence between the variational results and the MC simulations for the ground-state phase diagrams of H_2, we now proceed to describe the finite-temperature properties of the model using extensive Monte Carlo simulations. In order to retain the focus, we again refer to the similarities of the present model with those proposed for CuO. Therefore, for the remainder of the paper we focus on a parameter regime, which highlights this similarity.

C. Finite-temperature results: weakly coupled sublattices

If the hierarchy of the coupling strengths is such that $|J_{2a}| \sim |J_{2b}| >> |J_1| \sim |K'|$, then it is easy to see that the square lattice separates into two sublattices, which are interpenetrating each other, but are weakly coupled. In fact, for $K' = 0$ these sublattices are completely decoupled. While this situation appears only a theoretical possibility in the present model, as the nnn couplings are stronger than the nn couplings, it can be realized in 3D oxide structures where the strength and the sign of a superexchange interaction crucially depends on the locations of the bridging oxygens in the crystal structure. CuO presents one example, where not only Cu-O-Cu superexchange is important but also the Cu-O-O-Cu supersuperexchange contribution is significant.[32] Such a decoupling into two sublattices has been highlighted in tetragonal CuO, where the intrasublattice exchange parameters are almost six times larger than the intersublattice couplings.[56]

We begin by analyzing the effects of biquadratic coupling on the ground state in a simple variational picture. Let us assume that the vector order parameters of the decoupled sublattices make an angle θ with each other. This is schematically shown in Fig. 8 where solid (red) and dashed (blue) lines highlight the two sublattices. Within each sublattice the spins are arranged ferromagnetically along one diagonal and

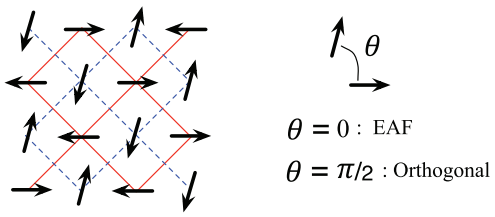

FIG. 8. (Color online) A schematic view of the decoupled magnetic sublattices that arise in the Heisenberg model given by H_0 in the limit of small nn coupling strength. Solid and dashed lines indicate the two sublattices. One can easily check that the ground-state energy does not depend on J_1 when the order within each sublattice is robust, hence any value of the angle θ between the sublattice order parameters corresponds to a magnetic ground state. Note that $\theta = 0$ and $\theta = \pi/2$ correspond to the collinear EAF state and the orthogonal spiral state, respectively.

antiferromagnetically along the other. The relative orientation of the spins on two sublattices is parameterized by angle θ. The ground-state energy of the system in the absence of biquadratic couplings is independent of θ, and hence there is a degeneracy of magnetic states in the system. The additional energy contribution due to the biquadratic coupling K' can be written as $E(\theta) = K' \cos^2\theta$. Minimizing the energy by demanding $dE/d\theta = 0$ and $d^2E/d\theta^2 > 0$, leads to two possible solutions: $\theta_{\min} = 0$ for $K' < 0$ and $\theta_{\min} = \pi/2$ for $K' > 0$. Therefore the introduction of a biquadratic coupling term lifts the degeneracy and stabilizes two specific phases, the EAF state or the orthogonal spiral state, depending on the sign of K'. These two phases are analogous to the AF_1 and AF_2 magnetic states of CuO. One of the interesting features in CuO is the existence of a noncollinear AF_2 magnetic state at high temperatures. This magnetic state supports a finite electric polarization due to its spiral nature and therefore is responsible for the high-temperature ferroelectric behavior of CuO. This is unusual as in most frustrated magnets, it is the low-temperature phase that supports a noncollinear magnetic phase and hence the ferroelectricity is observed only at low temperatures. Given the similarity of the present model with that of CuO, it is natural to ask if a spiral magnetic order exists at high temperatures within the present model.

In order to answer this, we compute a quantity P, which is proportional to the electric polarization induced via the inverse DM mechanism,[19] as a measure of the spiral nature of spin states. Following Katsura *et al*. we define P as,[19]

$$P = \frac{1}{N}\left\langle \left| \sum_i \mathbf{P}_i \right| \right\rangle$$
$$\mathbf{P}_i = \hat{\mathbf{x}} \times (\mathbf{S}_i \times \mathbf{S}_{i+\hat{x}}), \tag{13}$$

where the vertical bars denote the magnitude of the vector and the angular brackets denote thermal average. $|\mathbf{P}_i|$ can be regarded as a local measure of P on a given bond along the x direction originating at lattice site i. Instead of introducing another name for P, we will refer to it as electric polarization. Note that P is also related to the spin current,[57] as both quantities involve a cross product of the spin vectors on neighboring sites. Temperature dependence of the electric polarization P is shown in Fig. 9(a) for

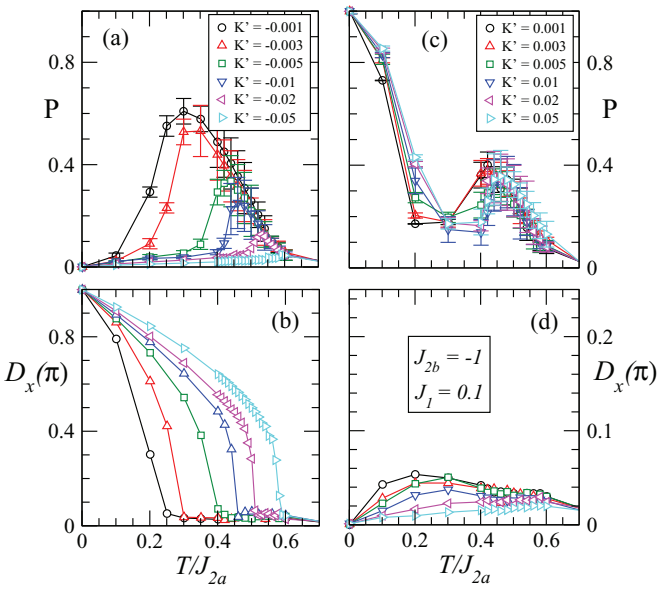

FIG. 9. (Color online) Temperature dependence of the electric polarization P for different values of K' in the range, (a) $K' < 0$ and (c) $K' > 0$. Temperature dependence of the order parameter $D_x(\pi)$ for the collinear magnetic state EAF for various values of K' in regimes, (b) $K' < 0$ and (d) $K' > 0$. Results are obtained on 120×120 lattice, with $J_1 = 0.1$ and $J_{2b} = -1$. Note the difference in scale on the y axis in (d).

negative values of K'. The Monte Carlo results are consistent with the variational analysis and P indeed vanishes at low temperatures. The high-temperature behavior is intriguing: there is a window in temperature where P becomes finite, indicating the existence of a noncollinear magnetic state at finite temperatures. Interestingly, the temperature range of stability of the noncollinear magnetic state increases upon decreasing the magnitude of K'. This suggests that the noncollinear phase may be entropy driven, as a large negative K' favors the collinear state and hence competes with the noncollinear state at high temperatures, narrowing the window of stability of the later state. We also notice that the electric polarization shows large fluctuations, which is the origin of relatively large error bars in Figs. 9(a) and 9(c).

Recalling the definition Eq. (13), we note that $D_x(\mathbf{Q})$ at $\mathbf{Q} = (\pi,\pi)$ [denoted as $D_x(\pi)$] is an order parameter for the EAF phase. $\mathbf{S}_i \cdot \mathbf{S}_{i+\hat{x}}$ represents the local degree of collinearity between neighboring spins along the x direction. Note that in the EAF phase, the dot product between neighboring spins have a perfect staggered order. This motivates the use of $D_x(\pi)$ as an order parameter for the EAF phase, much like the staggered magnetization is an order parameter for the AFM state. The temperature dependence of $D_x(\pi)$ is plotted in Fig. 9 (b) for $K' < 0$. The ground state is collinear as the order parameter rises smoothly to its maximal value upon reducing temperature in our simulations. The temperature at which $D_x(\pi)$ shows an abrupt rise, correlates well with the temperature at which the electric polarization begins to fall. Therefore, the temperature dependence of P and $D_x(\pi)$ can be used to assign characteristic temperatures at which the collinear and the spiral magnetic orders set in. Next, we study the behavior of the model for positive values of K'. In agreement with the variational results, the ground state supports a noncollinear order [see Fig. 9(c)]. $P = 1$ indeed corresponds to the orthogonal magnetic phase where neighboring spins point at an angle of 90° to each other. Therefore the transition between a collinear and noncollinear magnetic orders as a function of K' is well captured in our simulations. However, the finite-temperature behavior of the model is quite different for positive K'. The electric polarization shows a nonmonotonic dependence on temperature, which is similar for different values of K'. Upon increasing temperature P decreases smoothly from its maximum value and then shows a weak rise before decreasing again. The collinear order parameter does not show any considerable rise in the intermediate temperature range. For $N = 120^2$, we find that $D_x(\pi) \sim 0.02$ in the high-temperature PM state. The maximum value of $D_x(\pi)$ in Fig. 9(d) is only about two times larger. This is in sharp contrast with the behavior of spiral order parameter P, which in the negative K' regime shows a value about 30 times larger than that in PM state [see Fig. 9(a)]. Clearly, the collinear state is only energetically stable and exists at finite temperatures only when $K' < 0$. Therefore, our results suggest that the noncollinear phase at high temperatures is stabilized by entropic effects. This is in agreement with previous material-specific models for CuO.[29,30] However, our results show that these results are a general feature of a model where the standard Heisenberg term leads to a degeneracy of magnetic states, and the ground-state selection relies on weaker higher-order couplings. One clear advantage of the BLBQ model is that the competition is only between EAF and orthogonal spiral states. This is unlike the models invoking DM coupling and magnetocrystalline anisotropy where it is possible to stabilize a spiral phase with arbitrary $\mathbf{q}$ depending on the relative strengths of the DM coupling and anisotropy.[29]

One of the advantages of the real-space approach is that we can investigate the spatial character of the finite-temperature noncollinear magnetism. For this purpose, we plot the real-space snapshots of the local collinear and noncollinear order parameters, $\mathbf{S}_i \cdot \mathbf{S}_{i+\hat{x}}$ and P_i. For $K' < 0$, the ground state is the up-up-down-down type antiferromagnet which corresponds to $\theta = 0$ in Fig. 8 (denoted as EAF). The real-space pattern at finite temperature ($T = 0.4$) show regions with strong noncollinear spin order [see Fig. 10(a)]. For $K' > 0$, the ground state supports a perfect orthogonal spiral order, where neighboring spins make an angle of $\pi/2$ with each other. At finite temperatures, regions with weak spiral order are present as inferred from the real-space distribution of P_i [see Fig. 10(b)]. Figures 10(c) and 10(d) show the corresponding snapshots of the collinear order, $\mathbf{S}_i \cdot \mathbf{S}_{i+\hat{x}}$. Collinear order is absent at $T = 0.4$. While we only show P_i and $\mathbf{S}_i \cdot \mathbf{S}_{i+\hat{x}}$ for a single configurations here, we have verified that these are typical configurations for $T = 0.4$. These real-space patterns also highlight the asymmetry with respect to K' that we discussed earlier. While at low temperatures the sign of K' decides the nature of the ordered magnetic state, at finite temperatures it is the noncollinear state that dominates irrespective of the sign of K'. At finite temperatures there are many different configurations of spins that are involved in the final thermal average. The electric polarization shows strong fluctuations at intermediate temperatures as we noticed in Figs. 9(a) and 9(c). However, the energy as a function

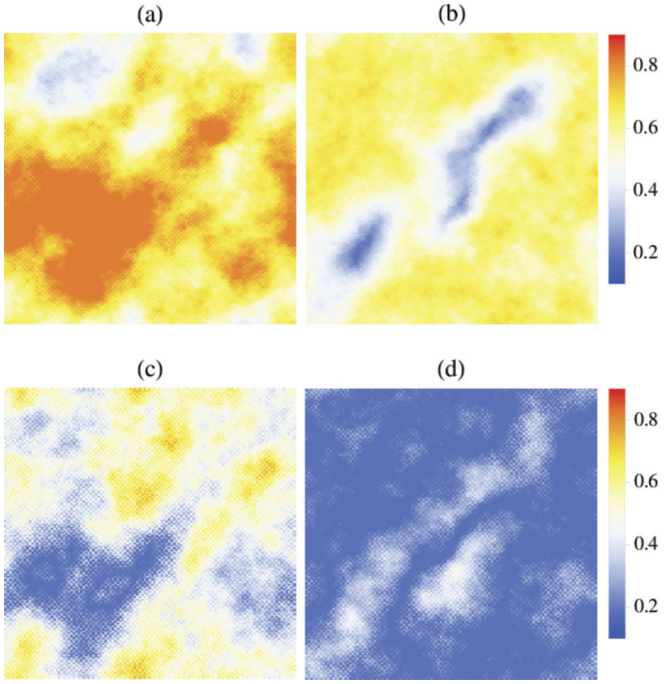

FIG. 10. (Color online) Real-space patterns of local measures for noncollinear and collinear orders, P_i (upper row) and $\mathbf{S}_i \cdot \mathbf{S}_{i+\hat{x}}$ (lower row), for $K' = -0.005$ [(a) and (c)] and $K' = 0.005$ [(b) and (d)] at intermediate values of temperature $T = 0.4$. These are single configurations that contribute to the averages plotted in Fig. 9.

of temperature (not shown) behaves smoothly with error bars less than the typical symbol size in our figures. Strong fluctuations in electric polarization with weak fluctuations in total energy indicate an unusual energy landscape in configuration space where many different configurations are present within a narrow energy range, and the system easily accesses these configurations. This explains why the spiral order wins over collinear order at finite temperatures: the availability of many different magnetic configurations with finite electric polarization increases the entropy of the system. Therefore, the system prefers to visit such configurations more often leading to a finite electric polarization. This highlights a key role of entropy in stabilizing the noncollinear magnetic order at finite temperatures. Moreover, our results suggest that the finite-temperature spiral phase is inhomogeneous. This compares favorably with recent experimental investigations, where the presence of an inhomogeneous ferroelectric phase in CuO has been reported.[52]

We summarize the results discussed in this section in a finite-temperature phase diagram. The Mermin-Wagner theorem prohibits a long-range magnetic order at finite temperatures for a classical continuous-spin model in 2D.[53,54] However, some of the magnetic phases discussed here break a discrete symmetry in addition to a continuous symmetry. In particular, the EAF state and the spin-spiral state both break the spatial inversion symmetry of the lattice. Therefore, finite-temperature phase transitions are allowed even in two dimensions for such magnetic phases.[55] While we have not carried out a thorough finite-size scaling analysis, numerical simulations on finite lattices can be used to identify characteristic temperatures at which the correlation length

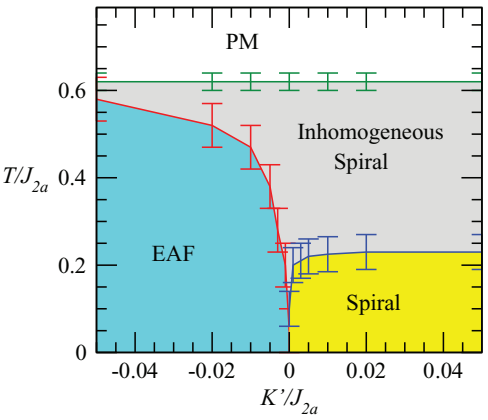

FIG. 11. (Color online) Temperature versus K' phase diagram for $J_{2b} = -1$ and $J_1 = 0.1$. The inhomogeneous spiral phase consists of islands of spiral phase coexisting with paramagnetic regions.

for a particular magnetic order exceeds the system size. The temperature dependence of $D_x(\pi)$ and P (as shown in Fig. 9) is used to identify such characteristic temperature scales for collinear EAF and spiral orderings, respectively. These are brought together as a phase diagram in Fig. 11. The ordering between the PM and the inhomogeneous spiral phase is independent of K'. This corresponds to the onset of ordering of the two sublattices (see Fig. 8), which is decided by the strengths of the couplings J_{2a} and J_{2b}. The inhomogeneous spiral phase corresponds to a state where PM regions coexist together with regions supporting large values of electric polarization. Upon reducing temperature further, the system orders into a collinear or noncollinear state depending on the sign of K'. The similarity of our results with those obtained on material-specific models for CuO is apparent.[29,30] The experimental situation of CuO is captured well in our model if we assume a small negative value of the biquadratic coupling K', where a window of stability of the noncollinear state exists between the collinear EAF and the fully disordered PM state. Our results suggest that this intermediate spiral phase contains inhomogeneities with patches of spiral patterns coexisting with magnetically disordered regions.

IV. CONCLUSIONS

We use a combination of variational calculations and Monte Carlo simulations to study a classical spin model on a 2D square lattice with nearest-neighbor and next-nearest-neighbor Heisenberg exchange interactions and nearest-neighbor biquadratic interactions. Motivated by the existence of a noncollinear magnetic state at high temperatures in CuO,[26] we study this model in a specific parameter regime where the nnn couplings are inequivalent and are much larger than the nn exchange interactions. In this limit, the system is decoupled into two sublattices and leads to a situation where even a weak biquadratic coupling is vital in selecting the ground-state magnetic order. We also compare the ground states of the BLBQ model with those of a model containing a four-spin ring-exchange coupling. It is the ring-exchange coupling that is physically relevant for a spin-1/2 system such as CuO. However, we demonstrate that the classical versions

of the quantum models for spin-1/2 and spin-1 have strong similarities in the parameter regime considered here. The finite-temperature study of the BLBQ model using Monte Carlo uncovers an inhomogeneous noncollinear magnetic state. The T-K' phase diagram of the model captures the main features of the phase diagrams reported in material-specific models for CuO, which considered the role of DM coupling and weak anisotropy. The present work helps in understanding the finite-temperature magnetism in CuO within a pure spin model in a general setting without taking into account the details of the crystal structure. We have shown that if the stronger interactions are such that they compete and lead to a degeneracy of magnetic ground states, then the role of the much weaker higher-order interactions cannot be ignored. These interactions are as important as other weak effects like the magnetocrystalline anisotropies and the spin-orbit induced DM interactions. Using the real-space analysis we also find that the high-temperature spiral phase is inhomogeneous with islands of spiral phase coexisting with paramagnetic regions. The common feature with the previous model studies is that the entropic effects are crucial in stabilizing the noncollinear state at high temperatures.[29,30] While there have already been some experimental reports that point to an inhomogeneous ferroelectric state in CuO,[52] it would be very interesting to probe further the spatial nature of the high-temperature noncollinear phase in CuO.

ACKNOWLEDGMENTS

The simulations were performed using the High Performance Computing Facility at IISER Mohali. We thank an anonymous referee for useful remarks and suggestions. K.P. acknowledges support from UGC-CSIR, India. S.K. acknowledges insightful discussions with Zohar Nussinov and Prabuddha Chakraborty, and financial support from DST, India.

[1] H. Schmid, Ferroelectrics **162**, 317 (1994).
[2] M. Fiebig, J. Phys. D: Appl. Phys. **38**, R123 (2005); N. A. Spaldin and M. Fiebig, Science **309**, 391 (2005); W. Eerenstein, N. D. Mathur, and J. F. Scott, Nature (London) **442**, 759 (2006).
[3] J. F. Scott, Nature Mater. **6**, 256 (2007).
[4] R. Ramesh and N. A. Spaldin, Nature Mater. **6**, 21 (2007).
[5] S. W. Cheong *et al*., Nature Mater. **6**, 13 (2007).
[6] F. Sugawara, S. Iida, Y. Syono, and S. Akimoto, J. Phys. Soc. Jpn. **25**, 1553 (1968).
[7] N. A. Hill and K. M. Rabe, Phys. Rev. B **59**, 8759 (1999).
[8] N. A. Hill, J. Phys. Chem. B **104**, 6694 (2000).
[9] N. A. Hill, Annu. Rev. Mater. Res. **32**, 1 (2002).
[10] D. I. Khomskii, J. Mag. Mag. Mat. **306**, 1 (2006); D. Khomskii, Physics **2**, 20 (2009).
[11] N. J. Perks, R. D. Johnson, C. Martin, L. C. Chapon, and P. G. Radaelli, Nature Commun. **3**, 1277 (2012).
[12] S. Ishiwata, Y. Kaneko, Y. Tokunaga, Y. Taguchi, T.-h. Arima, and Y. Tokura, Phys. Rev. B **81**, 100411(R) (2010).
[13] L. C. Chapon, G. R. Blake, M. J. Gutmann, S. Park, N. Hur, P. G. Radaelli, and S.-W. Cheong, Phys. Rev. Lett. **93**, 177402 (2004).
[14] T. Kimura, J. C. Lashley, and A. P. Ramirez, Phys. Rev. B **73**, 220401(R) (2006).
[15] S. Seki, Y. Onose, and Y. Tokura, Phys. Rev. Lett. **101**, 067204 (2008).
[16] S. Horiuchi and Y. Tokura, Nature Mater. **7**, 357 (2008).
[17] P. Lunkenheimer, J. Müller, S. Krohns, F. Schrettle, A. Loidl, B. Hartmann, R. Rommel, M. de Souza, C. Hotta, J. A. Schlueter, and M. Lang, Nature Mater. **11**, 755 (2012).
[18] J. van den Brink and D. Khomskii, J. Phys.: Cond. Mat. **20**, 434217 (2008).
[19] H. Katsura, N. Nagaosa, and A. V. Balatsky, Phys. Rev. Lett. **95**, 057205 (2005).
[20] M. Mostovoy, Phys. Rev. Lett. **96**, 067601 (2006).
[21] I. V. Solovyev, Phys. Rev. B **83**, 054404 (2011).
[22] C. Ederer and N. A. Spaldin, Phys. Rev. B **71**, 060401(R) (2005); I. A. Kornev, S. Lisenkov, R. Haumont, B. Dkhil, and L. Bellaiche, Phys. Rev. Lett. **99**, 227602 (2007).
[23] T. Kimura, Annu. Rev. Mater. Res. **37**, 387 (2007).
[24] L. N. Bulaevskii, C. D. Batista, M. V. Mostovoy, and D. I. Khomskii, Phys. Rev. B **78**, 024402 (2008).
[25] I. A. Sergienko and E. Dagotto, Phys. Rev. B **73**, 094434 (2006).
[26] T. Kimura, Y. Sekio, H. Nakamura, T. Siegrist, and A. P. Ramirez, Nature Mater. **7**, 291 (2008).
[27] M. Mostovoy, Nature Mater. **7**, 269 (2008).
[28] X. Rocquefelte, K. Schwarz, P. Blaha, S. Kumar, and J. van den Brink, Nature Commun. **4**, 2511 (2013).
[29] G. Giovannetti, S. Kumar, A. Stroppa, J. van den Brink, S. Picozzi, and J. Lorenzana, Phys. Rev. Lett. **106**, 026401 (2011).
[30] G. Jin, K. Cao, G.-C. Guo, and L. He, Phys. Rev. Lett. **108**, 187205 (2012).
[31] P. Toledano, N. Leo, D. D. Khalyavin, L. C. Chapon, T. Hoffmann, D. Meier, and M. Fiebig, Phys. Rev. Lett. **106**, 257601 (2011).
[32] X. Rocquefelte, K. Schwarz, and P. Blaha, Sci. Rep. **2**, 759 (2012).
[33] J. B. Forsyth, P. J. Brown, and B. M. Wanklyn, J. Phys. C: Solid State Phys. **21**, 2917 (1988).
[34] B. X. Yang, T. R. Thurston, J. M. Tranquada, and G. Shirane, Phys. Rev. B **39**, 4343 (1989).
[35] K.-Y. Choi, W.-J. Lee, A. Glamazda, P. Lemmens, D. Wulferding, Y. Sekio, and T. Kimura, Phys. Rev. B **87**, 184407 (2013).
[36] K. Cao, G.-C. Guo, D. Vanderbilt, and L. He, Phys. Rev. Lett. **103**, 257201 (2009).
[37] A. Kalz and G. Y. Chitov, Phys. Rev. B **88**, 014415 (2013).
[38] K. I. Kugel and D. I. Khomskii, Sov. Phys. Usp. **136**, 621 (1982).
[39] J.-Y. P. Delannoy, A. G. Del Maestro, M. J. P. Gingras, and P. C. W. Holdsworth, Phys. Rev. B **79**, 224414 (2009).
[40] F. Mila and F.-C. Zhang, Eur. Phys. J. B **16**, 7 (2000).
[41] C. Griset, S. Head, J. Alicea, and O. A. Starykh, Phys. Rev. B **84**, 245108 (2011).
[42] Y.-W. Lee and M.-F. Yang, Phys. Rev. B **85**, 100402 (2012).
[43] R. Singer, F. Dietermann, and M. Fähnle, Phys. Rev. Lett. **107**, 017204 (2011).
[44] Y. Kamiya, N. Kawashima, and C. D. Batista, Phys. Rev. B **82**, 054426 (2010).

[45]S. E. Korshunov, F. Mila, and K. Penc, Phys. Rev. B **85**, 174420 (2012).
[46]N. Shannon, K. Penc, and Y. Motome, Phys. Rev. B **81**, 184409 (2010).
[47]P. Corboz, A. M. Läuchli, K. Totsuka, and H. Tsunetsugu, Phys. Rev. B **76**, 220404(R) (2007); A. Läuchli, G. Schmid, and S. Trebst, *ibid*. **74**, 144426 (2006); J. Lou, T. Xiang, and Z. Su, Phys. Rev. Lett. **85**, 2380 (2000); K. Okunishi, Phys. Rev. B **60**, 4043 (1999).
[48]M. E. J. Newman and G. T. Barkem, *Monte Carlo Methods in Statistical Physics* (Oxford University Press, Oxford, 1999).
[49]N. Metropolis, A. W. Rosenbluth, M. N. Rosenbluth, A. H. Teller, and E. Teller, J. Chem. Phys. **21**, 1087 (1953).
[50]J. M. Luttinger and L. Tisza, Phys. Rev. **70**, 954 (1946); T. A. Kaplan and N. Menyuk, Philos. Mag. **87**, 3711 (2006).
[51]K. Harada and N. Kawashima, Phys. Rev. B **65**, 052403 (2002); B. A. Ivanov and A. K. Kolezhuk, *ibid*. **68**, 052401 (2003); A. Läuchli, F. Mila, and K. Penc, Phys. Rev. Lett. **97**, 087205 (2006); H. Tsunetsugu and M. Arikawa, J. Phys. Soc. Jpn. **75**, 083701 (2006).
[52]W. B. Wu, D. J. Huang, J. Okamoto, S. W. Huang, Y. Sekio, T. Kimura, and C. T. Chen, Phys. Rev. B **81**, 172409 (2010).
[53]N. D. Mermin and H. Wagner, Phys. Rev. Lett. **17**, 1133 (1966); P. C. Hohenberg, Phys. Rev. **158**, 383 (1967).
[54]A. Gelfert and W. Nolting, J. Phys.: Cond. Matt. **13**, 505 (2001).
[55]J.-H. Park, S. Onoda, N. Nagaosa, and J. H. Han, Phys. Rev. Lett. **101**, 167202 (2008).
[56]G. Peralta, D. Puggioni, A. Filippetti, and V. Fiorentini, Phys. Rev. B **80**, 140408(R) (2009).
[57]K. A. Al-Hassanieh, C. D. Batista, G. Ortiz, and L. N. Bulaevskii, Phys. Rev. Lett. **103**, 216402 (2009).